Available online at www.academicpaper.org

Academic @ Paper

ISSN 2146-9067

International Journal of Automotive Engineering and Technologies

Vol. 4, Issue 2, pp. 68 – 81, 2015

International Journal of Automotive Engineering and Technologies

http://ijaet.academicpaper.org/

Original Research Article

Material Selection for Dynamic Variable Geometry Turbocharger Flow Control Application

Apostolos Pesiridis[1*], Srithar Rajoo[2], Kishokanna Paramasivam[2], Ricardo Martinez-Botas[3] and Robert Macnamara[4]

[1]School of Engineering and Design, Brunel University London
[2]Transport Research Alliance, Universiti Teknologi Malaysia
[3]Department of Mechanical Engineering, Imperial College London
[4]BP, Houston, TX, 77079, USA

Receive 02 April 2014, Accepted 25 June 2015

Abstract

This paper investigates nozzle material candidates for use in a turbocharger turbine technology known as the active control turbocharger (ACT) which is a distinct technology to the Variable Geometry Turbine (VGT) for turbochargers, but broadly based on this technology. In this concept an actuated nozzle mechanism is oscillated to provide a continuous change of the turbine inlet area in response to the instantaneous exhaust gas flow pulsating characteristics to provide greater extraction of exhaust gas pulse energy. Careful materials selection is required for this application to overcome the creep, fatigue, oxidation and high temperature challenges associated with the diesel engine exhaust conditions to which the nozzle is exposed to. The investigation of materials suitability for this application was conducted for steady and transient flow conditions. It was found that the nozzle vane undergo cyclical loading at a maximum stress of 58 MPa for 10^9 cycles of operation at an inlet temperature of 800°C and pressure of 240 kPa. The vane experiences maximum stresses in the closed position which occurs at a vane angle of 70°. It has been found that the implementation of ACT technology is possible using currently available materials. A material selection process was developed to incorporate the specific application requirements of the ACT application. A weightinG decision process was applied to analyse the importance of various material properties to each application requirement and to the properties of individual materials. Nimonic 90 and IN X750/751 obtained the highest overall scores from the selection process and were shown to be capable of withstanding the creep requirements; a failure mechanism of primary concern in the high temperature application. Nimonic 80A, although receiving a final rating 8% lower than Nimonic 90, also showed promising potential to offer a solution, with superior corrosion properties to both Nimonic 90 and IN X750/751.

Keywords: Variable Geometry Turbocharger, Active Control Turbocharger, superalloys, pivoting vane, CFD, FEA, transient analysis

Nomenclature

ACT	Active Control Turbocharger		turbine entry
CFD	Computational Fluid Dynamics	C	number of cylinders
FEA	Finite Element Analysis	θ	angle position (degree)
VGT	Variable Geometry Turbine (Turbocharger)	T	torque
		I	moment of inertia
f	frequency	α	angular acceleration
N	revolution per minute	£	pounds sterling (currency)
n	number of strokes		
G	number of groups connected to the		

*Corresponding author:
apostolos.pesiridis@brunel.ac.uk

1. Introduction

In the current decade, the European automotive industry must reduce the average emissions levels of light vehicles by 32% to meet the 2020 target of 95 gCO_2/km as mandated by EC regulation No. 443 (European Commission, 2010). Developments in turbocharger technology are of particular interest to meet these reductions, due to their ability to improve drivability and power output while improving fuel consumption and decreasing emissions (Pesiridis, 2007).

Turbochargers for gasoline and diesel engines capture energy from exhaust gases to improve power output and contribute to engine downsizing. Upon leaving the engine cylinders, the hot exhaust gas is channelled through the turbocharger turbine (Fig.1). The turbine shaft is connected to a compressor located upstream of the engine intake manifold. As the exhaust gas drives the turbine and through it the compressor, the latter is able to draw additional air into the engine cylinders. The higher density of air in the cylinders allows more fuel to be combusted and thus, more power is achieved with each stroke.

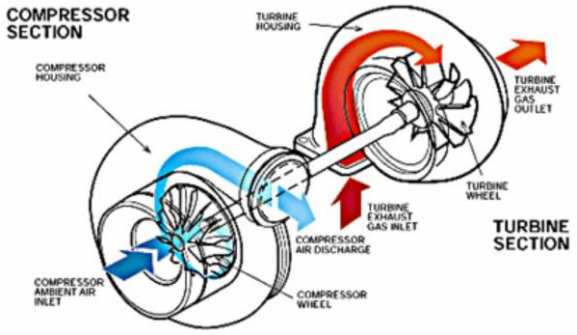

Figure 1: Schematic of main turbocharger components (Pesiridis, 2007)

Despite their benefits, it has been found that current turbocharger technologies fail to fully capture the highly dynamic energy of the pulsating exhaust gas flow (Pesiridis and Martinez-Botas, 2006). As such, Pesiridis and Martinez-Botas (2007) introduced the concept of the Active Control Turbocharger (ACT) whereby the effective throat area of the turbine is continually modulated by means of a fast-response nozzle. In their work, it was demonstrated that ACTs yield an improvement in power between 3-7% compared to standard VGTs. This enhanced energy recovery capability allows the ACT to potentially bring about greater engine weight reduction, lower fuel consumption and improved performance compared to currently available turbochargers.

In the ACT, the inlet area to the turbine rotor is adjusted in accordance with the incoming pressure pulses. This ideally would results in a uniformly smoother pressure field applied to the rotor allowing for improved power output and efficiency if the appropriate level of instantaneous inlet area can be provided in a timely manner. To allow modulation of the nozzle (rack) position per incoming exhaust pulse, the nozzle must be able to oscillate at high frequencies which for this study were limited to 50 Hz as representative engine operating frequency (speed) and against a transient flow of exhaust gas at high temperatures between 850 – 1050°C depending on engine type (Honeywell, 2010). Rajoo (2007) extended the concept of ACT to include a more conventional ring of pivoting vanes for the nozzle around the circumference of the rotor. The intended application of ACT for this project was a 10 litre, Diesel engine where Rajoo's pivoting vane system was put to the test (Rajoo, 2007) and around which this study is concentrated.

The conditions of operation faced by these vanes are extreme and, given the rapid oscillation, unlike any other application currently found in turbocharger or gas turbine technology. The high-temperature, high-frequency operation compounded with the mechanical stress applied by the actuating mechanism and the oxidizing environment of the transient exhaust gas pulses impose significant limitations on the materials that can be used in the manufacturing of these vanes. As such, effective materials selection for these components is of utmost importance and requires comprehensive understanding of the stresses experienced by the mechanism through the most representatively extreme operating conditions for this application.

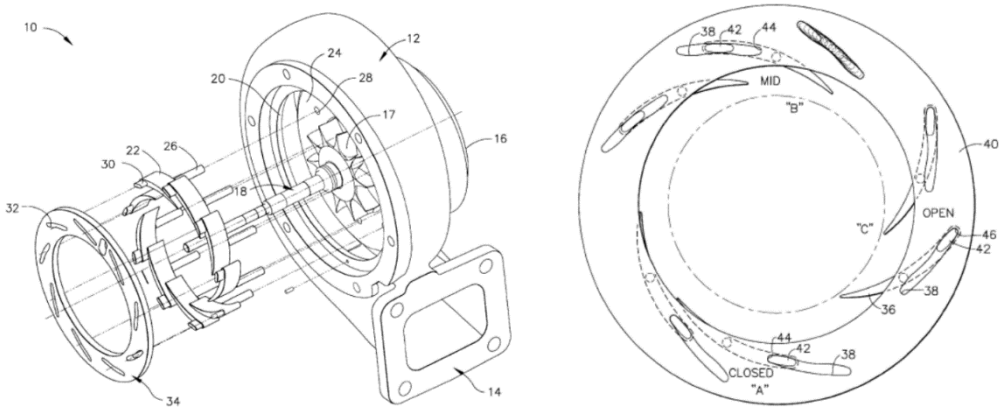

Figure 2. Pivoting Vane Mechanism (a) Isometric exploded view (b) Different positions of the vane (Arnold, 2004)

This paper focuses on identifying the materials that can withstand the high cycle life times, temperatures and stresses involved in ACT operation through aerodynamic flow simulation to obtain the mechanical forces and resulting stresses acting on the nozzle vane mechanism.

2. The Pivoting Vane Mechanism in Active Control Turbocharger

The pivoting vane nozzle and sliding nozzle mechanisms currently employed in VGT use operate in response to engine conditions rather than the high-frequency exhaust pulse response required by ACT. Fig.2 shows a simplified diagram of pivoting vane mechanism. The vanes are actuated open and closed by a rotating disc in order to control the flow of exhaust across the turbine (Arnold, 2004).

In ACT operation, the vanes rapidly oscillate between the 40° (open position) and 70° (closed position) vane angles to adjust the rotor inlet area in accordance with the gas pulse (Rajoo, 2007). The intermediate position is described by an angle of 55°.The frequency of oscillation representing the engine rotational speed depends on the size and type of the engine is provided by Equation (1) below:

$$f = \frac{2NCG}{60n} \qquad (1)$$

Where f is the frequency of emitted exhaust pulses and is dependent on engine speed N (rpm), n, is the number of strokes, G, the number of groups connected to the turbine entry and C, the number of cylinders. Fig.3 illustrates the angular position as a function of time based on this frequency of operation, assuming a sinusoidal variation described by Equation (2):

$$\theta = (\pi/12)\sin(50(2\pi t)) \qquad (2)$$

Equation (2) is obtained simply by treating the 55°position as the neutral position, corresponding to an angle of 0 radians, and the 70° and 40° positions as +/- π/12 radians, respectively.

Below is outlined a method of calculating the torque necessary to achieve the oscillation. The procedure begins with the simple equation that describes torque as a product of the moment of inertia, I, and the angular acceleration, α, as described by Equation (3):

$$T = I\alpha \qquad (3)$$

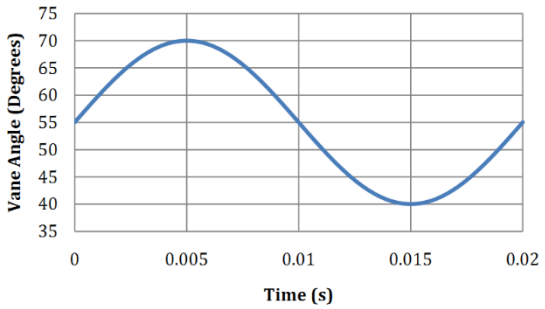

Figure 3: Sinusoidal variation of vane angle with time

With angular acceleration calculated from the second derivative of angular position, θ (Equation (2)) resulting in Equation (4):

$$\alpha = (100\pi)^3/12)(-\sin 50(2\pi t)) \qquad (4)$$

Hence the final equation with torque as a function of time is described by Equation (5).

$$T = I((2fn)^3/12)(-\sin 50(2\pi t)) \qquad (5)$$

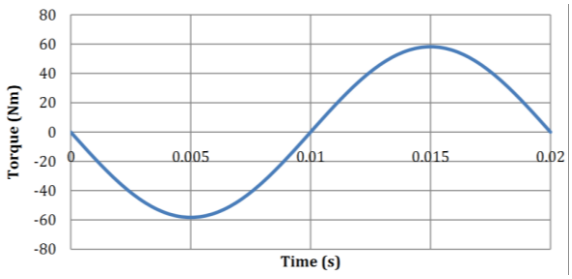

Figure 4: Variation of torque with time

3. Internal Combustion Engine Operating Conditions

The raw data used for this work is based on a 10-litre diesel engine operating at 2000 rpm which provided a worst-case scenario in terms of emitted pulse frequency. The raw data was obtained from a previous model of this engine and are given in Figures 5-7. This data was then used as boundary conditions for the computational analysis detailed in Section 5.

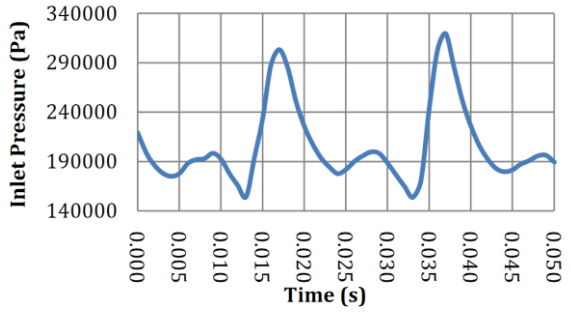

Figure 5: Raw data of pressure pulse

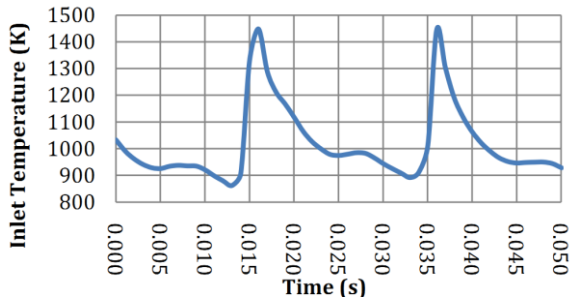

Figure 6: Raw data of temperature pulse

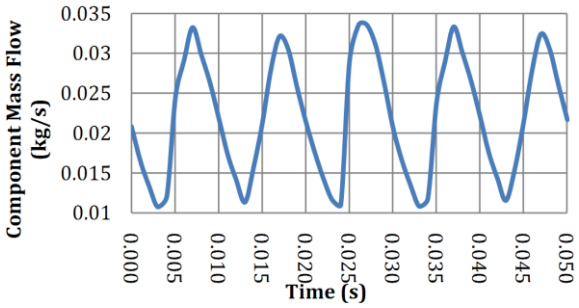

Figure 7: Raw data of mass flow pulse

4. Materials Analysis

The environment of the internal combustion engine in which the ACT vanes are required to operating in is characterized by:

1. High temperature fluctuations
2. High-pressure fluctuations
3. Transient flow of corrosive combustion products such as H_2O, CO_2 and nitrous oxides (Munz et al, 2007)

Hence, the selected material must be able to withstand these extreme conditions without failure. Failure refers to the component no longer being capable of carrying the required load and fails by fracture or other failure mechanism. Farag (2008) and Mazur (2005) have described several modes of failure for components operating under such conditions:

a) Yield failure
b) Creep failure
c) Thermal and Mechanical fatigue
d) Oxidation

As a consequence of the listed material failure mode, the focus of this work is with the high performance group of alloys known as superalloys, which are capable of retaining their physical and micro-structural properties at elevated temperatures. The reason for the selection of superalloys will become apparent through a study of their characteristics in the next section.

4.1 The Superalloys

A review of the literature shows that the following materials are currently under investigation for application in the various turbocharger components:

- Stainless Steels (Farag, 2008)
- Superalloys (Jovanovic, 2004, Shouren, 2008, Tetsui, 1999)
- Titanium -aluminum alloys (Jovanovic, 2004, Shouren, 2008, Tetsui, 2002, Zhang, 2001)
- Silicon nitride-based ceramics (Bocanegra-Bernal, 2010, Jovanovic, 2004)
- Refractory Metals (Farag, 2008)

Figure 8 compares the oxidation and temperature strength of several of these

classes of materials. It is seen that some refractory metals are stronger at higher temperatures but lack the ability to operate in oxidizing conditions. Titanium-aluminium alloys and ceramics are not displayed in Figure 9 but they are under development due to their advantage of having a much lower density than the superalloys (Bocanegra-Bernal, 2010; Shouren, 2008). However, these materials are in the development stage with a resultant high cost of manufacture and limited industry experience; for these reason they have been excluded from the present study but could become an option in the future. Thus, nickel-based superalloys appear to be the most appropriate materials for consideration for application in ACT nozzle.

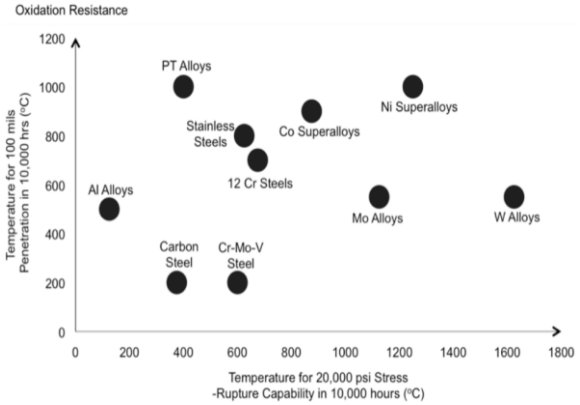

Figure 8. Relative capabilities of alloy systems (Sims, Stoloff & Hagel, 1987)

4.2 Material Properties

With the primary failure mechanisms having been identified in the previous section, Table 1, below, summarises the principal data associated with the failure mechanisms that will be used as a basis for comparison in the material selection process.

Table 1: Corresponding properties of materials directly related to likely failure mechanisms (Dieter, 1997)

Failure Mechanism	Ultimate Tensile Strength	Fatigue	Creep Rate	Coefficient of Thermal Expansion	Electrochemical Potential
Creep			X		
Low Cycle Fatigue		X			
High Cycle Fatigue	X	X			
Corrosion					X
Thermal Fatigue			X	X	

It is seen that the ultimate tensile strength (UTS), fatigue stress, creep rate, thermal expansion coefficient (CoTE), and electrochemical potential are the most important parameters to explore for the

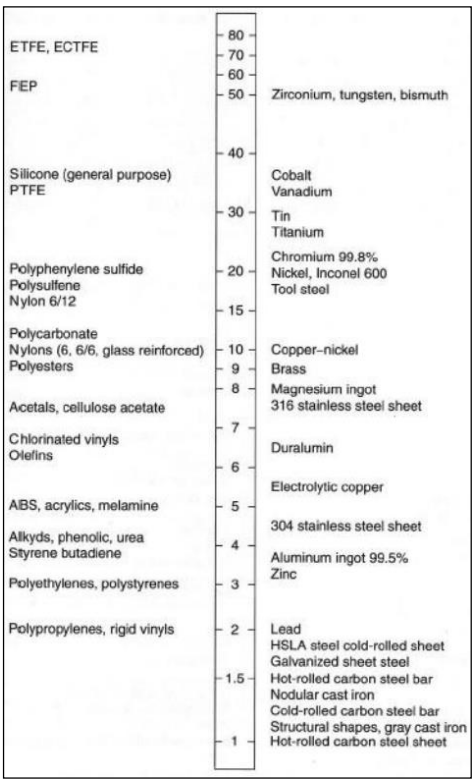

Figure 9. Cost comparison of various materials on a per unit mass basis. Comparison is made relative to the cost of hot-rolled low-carbon steel sheet (Farag, 2008).

Table 2: Reasons for selection of material for ACT vane assembly

MATERIAL	REASONS/ADVANTAGES
Inconel 600	Standard engineering material for applications requiring corrosion and heat resistance. It is not precipitation hardenable but is strengthened only by cold work. (Special Metals Corporation, 2002).
Inconel X-750/751	IN X750 and 751 have similar properties and compositions and are found primarily in internal combustion engine exhaust systems. Unlike IN 600, these materials are hardened through precipitation of the gamma phase (Special Metals Corporation, 2004).
Inconel MA754	An oxide dispersion strengthened nickel-chromium superalloy with high creep resistance and a very different composition to the preceding materials (Special Metals Corporation, 2004)
CMSX-4	Second-generation single crystal nickel alloy with the highest creep resistance of the metals compared. (The C-M Group, 2004)
Nimonic 80A/81/90	These materials are easier to fabricate and have similar properties to IN X750/751. Practical for the detail and size of the components required for the ACT vanes.

application of interest in this work. Such parameters have been the basis for material selection in several reviews (Ashby, 1992, Dieter, 1997) covering the performance of components in similar high temperature conditions.

Based on an iterative process to analyse each of the material properties, several nickel-based superalloy materials were selected as the candidates. The materials are Inconel 600, Inconel X-750, Inconel 751, Incoloy 864, Nimonic 80A,81 and Nimonic 90. Table 2 provides the principal characteristics and

main areas of application of the selected materials and therefore the reason for their inclusion in the present study.

5. Computational Analysis

The study to characterise the levels of stress experienced by each nozzle vane consisted of a combination of Computational Fluid Dynamics (CFD) and Finite Element Analysis (FEA). The ANSYS CFD (CFX) and ANSYS FEA packages were utilised for the simulations. The first step involved an aerodynamic analysis of the vane to characterise the surrounding fluid flow and resulting pressure and temperature profile on the vane surface. Subsequently, FEA was initiated to calculate the resulting stress on the vane. Finally, a material analysis is performed where the resulting stress is compared to manufacturer data sheets to assess how different materials would perform under the prescribed conditions. Figure10 shows the fluid domain of the pivoting vanes at angles of 40, 55 and 70 degrees (maximum, intermediate and minimum positions, respectively). The inwards-facing vectors outline the inlet boundary surface, with the outwards-facing vectors outlining the outlet boundary surface. These domains are repeated axisymmetrically around the Z-axis, to account for the total of 15 vanes. The axisymmetric assumption allows the analysis to be performed on only one vane, rather than creating a fluid domain incorporating all 15 vanes and thus allowing for an efficient computational analysis to be performed.

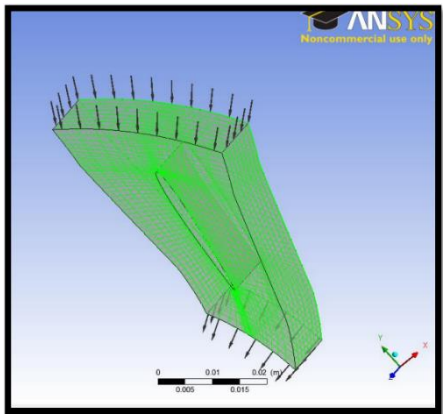

Figure 10. Fluid Domain describing the vane at angular position of 40°

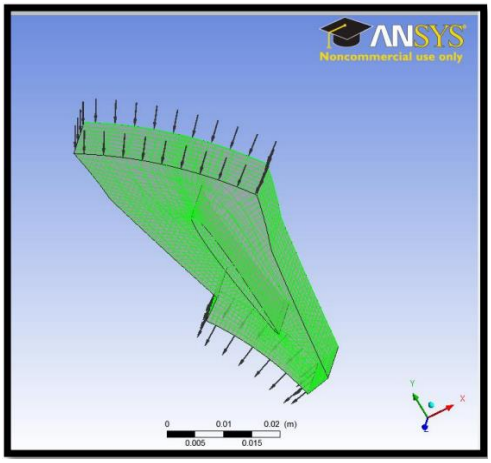

Figure 11. Fluid Domain describing the vane at angular position of 55°

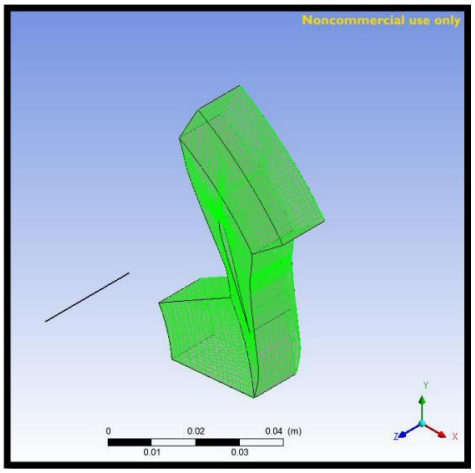

Figure 12. Fluid Domain describing the vane at angular position of 70°

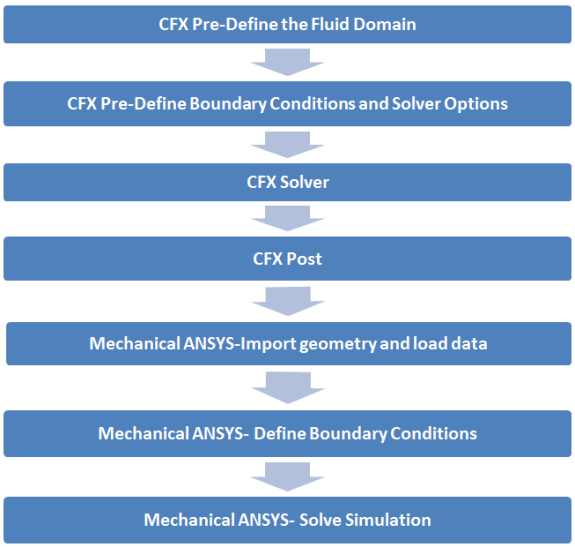

Figure 13. Flow diagram illustrating the step by step process used to execute the CFD and FEA simulations

5.1 Transient Study

Ideally, a transient study would need to be carried out where a moving fluid domain

would be applied that replicated the vane angle oscillation with time dependent boundary conditions defined to match the correct timing of the angular position. However, the complexity of generating a moving fluid domain sufficient to achieve this was deemed to be of sufficiently large complexity and of such time-intensity as to render this undertaking unrealistic within the project constraints. This meant that simplifications and approximations had to be made to best replicate actual conditions as much as feasible.

The method employed in this study required three fluid domains to be identified, describing three different angular positions. Applying a whole period of raw data from one exhaust pulse to be used for each of these angles would lead to unnecessarily long simulation times and post processing. To avoid this, it was assumed that a small number of discrete domains was adequate to replicate the sinusoidal trace of the pulse. Figure 14 shows how the allocation of these sections was split between the three domains.

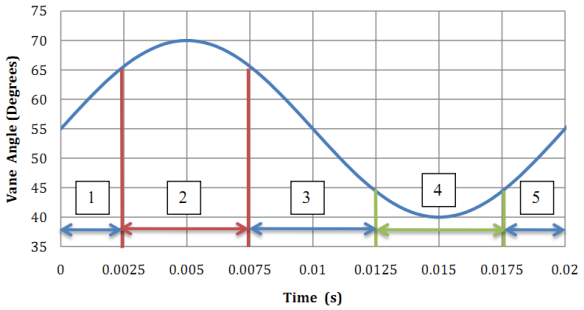

Figure 14: Transient study approach

The domain of the 40° vane angle is assumed to sufficiently describe the time bounded by vertical green lines on Figure 14 (angle of 40° – 45°), with the domain of the 70° vane angle assumed to sufficiently describe the time bounded by the vertical red line (angles of 65° – 70°). The remainder of the time within the period of 0.02s, represented by the blue lines which is assumed to bound by the angle 55° vane angle (angles of 45° – 65°). A separate transient study was run for each of the five segments shown in Figure 14. This required running an initial steady-state simulation for each of the segments to correctly initialise each transient simulation. Table 3 outlines the important data that was used to define each initial, steady-state simulation.

Table 3: Transient simulation initial steady state boundary conditions

Simulation Reference Number	Time Segment	Fluid Domain	Initial Mass Flow (kg/s)	Initial Temperature (K)	Initial Pressure (Pa)
1	0.0000-0.0025s	55^0	0.0208	1032.97	219228
2	0.0025-0.0075s	70^0	0.0118	949.50	181148
3	0.0075-0.0125s	55^0	0.0316	936.23	191685
4	0.0125-0.0175	40^0	0.0127	870.58	159880
5	0.0175-0.020s	55^0	0.0319	1234.23	296486

5.2 Mechanical-Structural Study

The structural analysis, although the most important output of the process, was in fact relatively simple to set up in comparison to the CFD setup in CFX. With the loading profile applicable to the blade already established, it was simply a matter of importing the geometry and correctly assigning the boundary conditions summarised in Table 4 to complete the process. The final step was to select the outputs required by the solver, in this case equivalent stress, and to evaluate the results.

Table 4: Mechanical ANSYS boundary conditions

Load Type	Description	Location
Rotational Support	Rigid Body Motion	Pivot Shaft
Torque	$T = I\frac{(2f\pi)^3}{12}(-sin(2f\pi t))$	Pivot Shaft
Blade Load	Load data calculated in *Solver*	Vane Surface

6. Results

6.1 Simulation "1" Results (55°)

Simulation "1" analysed the pivoting vane angle of 55° using the raw data corresponding to a time segment of between 0s and 0.0025s. The area of maximum stress illustrated in Figure 15 occurred at 40% of chord length (from the leading edge) while Figure 16 describes the time dependent variations of maximum equivalent stress and pressure difference. The stress variation at this position is best described by the change in pressure difference between the pressure and suction sides at the same location. The stress contours indicate that a maximum value of 4.12 MPa occured for a very concentrated area of the vane and that the global stresses experienced are closer to a value of 1-2 MPa. It is important to note that the entire range of maximum stress spans approximately 0.8 MPa. It will be seen in the

proceeding analyses that this is a relatively insignificant variation in stress in comparison to that which occurs throughout the whole time period of 0.02s.

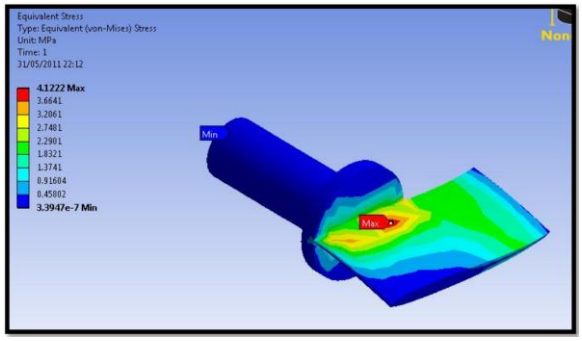

Figure 15: Equivalent stress contours for Simulation '1'

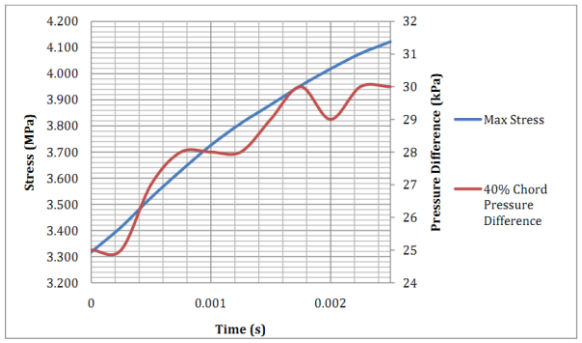

Figure 16: Maximum stress and 40% chord pressure difference variations with time output by CFX Solver and Post for Simulation '1'

6.2 Simulation "2" Results (70°)

Simulation '2' evaluates the raw data occurring between 0.0025s and 0.0075s for a 70° vane angle position. Figure 17 illustrates the geometric variation of stresses obtained during this time period, with a maximum value of 58.04 MPa located at approximately 60% chord and global stresses closer to 25-30 MPa. Figure 18 indicates the variation of maximum stress and pressure difference at 60% chord with respect to time. The variations of the maximum stress are greater than that seen in Simulation '1'and this can be attributed to the increased angle at which the vane is positioned relative to the flow i.e. the closed position. With the vane positioned to increase restriction of the flow, the effective area seen relative to the flow becomes greater than that seen by the 70° position, resulting in a higher level of stress. In addition, the much greater pressure differentials obtained between the pressure and suction sides, with a maximum value of 100 kPa, in comparison to 30 kPa seen in the previous simulation.

From Figure 18, the maximum stresses between 0.0025 and 0.0075 s can be represented by an average stress of 45 MPa. However, as the effect of vane angle has been shown to exert a strong influence on the aerodynamic and structural conditions experienced by the vane, this decrease in reality. The assumption that the vane is positioned at 70° for the entire duration is incorrect, as the vane oscillates between 65° and 70° during this time period.This means the calculated stresses either side of the maximum vane angle should theoretically decrease, minimising the average stresses present between 0.0025-0.0075 s.

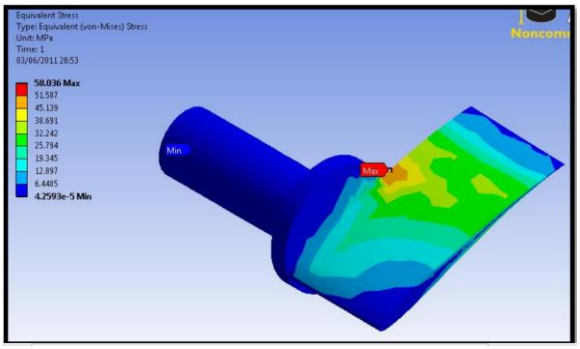

Figure 17: Equivalent stress contours for Simulation '2'

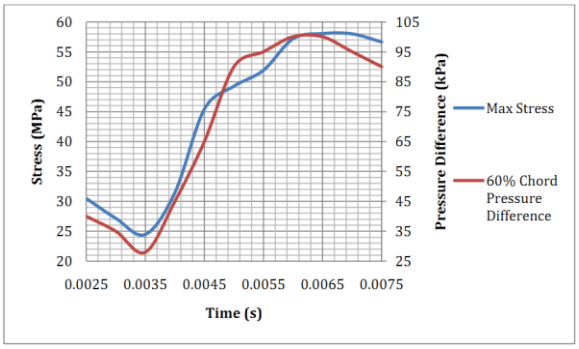

Figure 18: Maximum stress and 60% chord pressure difference variations with time output by CFX Solver and Post for Simulation '2'

6.3 Simulation "3" Results (55°)

Simulation '3' analyses the pivoting vane at an angle of 55° using the raw data corresponding to a time segment of 0.0075-0.0125s. Figure 19 illustrates the global stresses experienced by the vane at the most extreme condition during the 0.0075-0.0125

s time period. The maximum stress experienced is 4.91 MPa, with global stress in the 1-3 MPa range. The maximum stress variation followed the trend obtained in Simulation '1' with regards to a dependence on the pressure difference variation at the location of maximum stress, also described by Figure 20 and again at a location of 40% chord. Again, the maximum stress experienced is relatively small in comparison to the conditions elsewhere and should not pose a significant mechanical integrity concern for the vane.

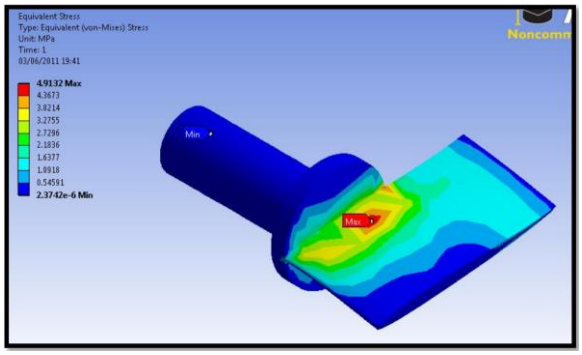

Figure 19: Equivalent stress contours for Simulation '3'

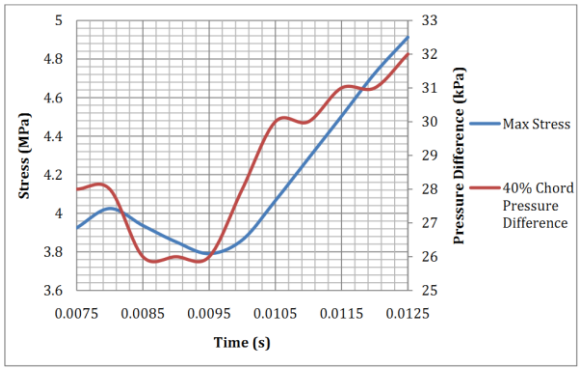

Figure 20: Maximum stress and 40% chord pressure difference variations with time output by CFX Solver and Post for Simulation '3'

6.4 Simulation "4" Results (40°)

Simulation '4' refers to the analysis that used the raw data corresponding to a time range of 0.0125-0.175s at a vane angle of 40°. The maximum pressure, located along the pressure side, remains relatively constant up to a chord length of approximately 60% with the maximum stress occurring between 2.8-5.6 MPa. This is a deviation from the trend exhibited by the 55° and 70° vane cases, where the stress variation is predominately a function of pressure difference and is a consequence of the vane being positioned at its 'most open' position and therefore being more aligned to the absolute angle of the incoming exhaust gases. The magnitude and range of maximum pressure experienced in this period of time is much greater than that seen by 55° vane, with Figure 22 describing a variation of approximately 140 kPa.

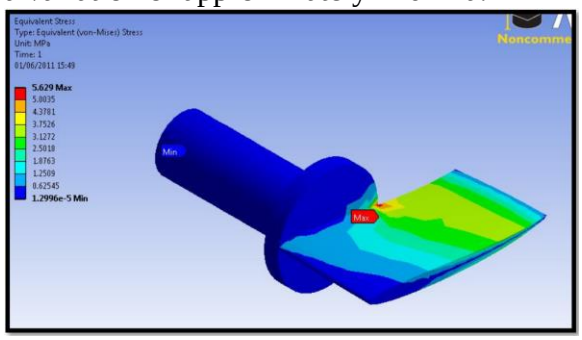

Figure 21: Equivalent stress contours for Simulation '4'

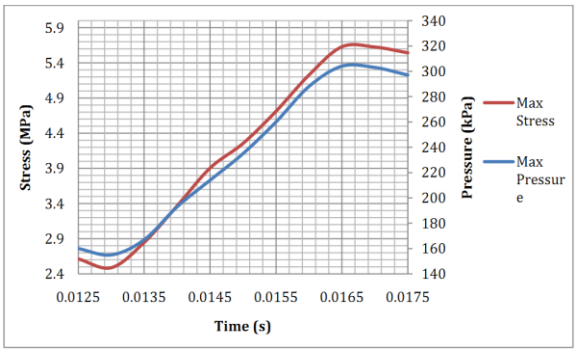

Figure 22: Maximum stress and 60% chord pressure difference variations with time output by CFX Solver and Post for Simulation '4'

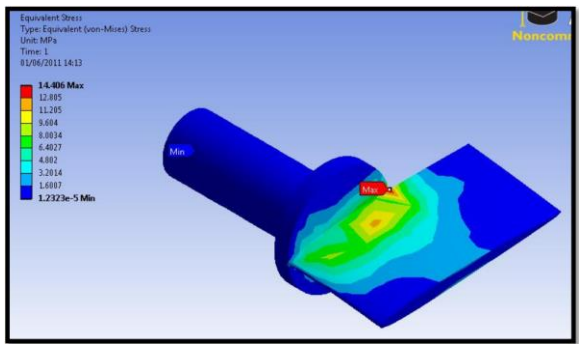

Figure 23: Equivalent stress contours for Simulation '5'

6.5 Simulation "5" Results (55°)

The final simulation reviews the results for the 0.0175-0.02s of the pulse period at a vane angle of 55°. Figure 23 illustrates the maximum stress variation, which in this instance occurs at 60% chord length, unlike the previous two simulations involving the

same 55° vane position; however, it can be seen there still exists an area of relatively high stress at 40% of chord length.

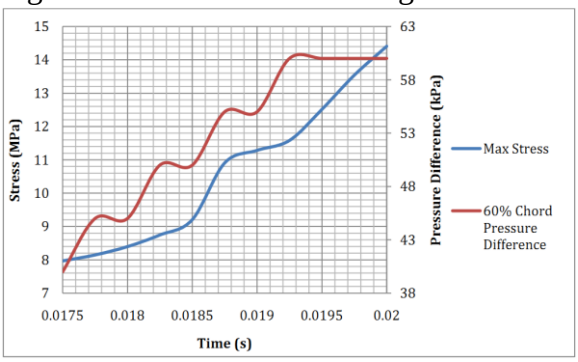

Figure 24: Maximum stress and 60% chord pressure difference variations with time output by CFX Solver and Post for Simulation '5'

6.6 Summary of the Simulation Results

In an attempt to demonstrate the general conditions experienced over the whole period, Figure 25 shows both the raw data obtained in Simulations '1' to '5' along with a prediction of the actual maximum stresses that would occur based upon the results discussed earlier. The trend line accounts for the three angular positions discussed and as already discussed the effect of angular position has been shown to have a significant impact on the conditions experienced. The simulation data is most accurate at time points of 0, 0.005, 0.01, 0.015 and 0.02s, when the vane angle and raw conditions match exactly. The trend line was therefore set to match the simulation data as much as possible at these points for a more accurate characterisation of the vane stress variation over the pulse period.

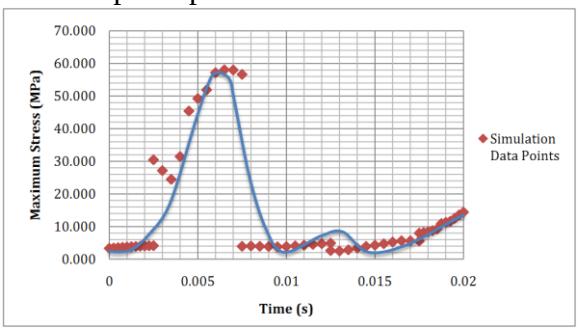

Figure 25: Maximum stress predictions based upon simulation outputs for entire time period of 0.02 s

7. Material Selection Process and Recommendations

A material selection process should aim to remove as much bias that the operator may have towards certain materials. A useful step in achieving this is to remove evaluation of a specific materials' suitability from the first stage of the process and instead evaluate only the importance of different material properties. A further extension of this is to relate these properties to the specific application of concern, in this case the pivoting vane ACT device. This has the advantage of forcing the developer to justify the decision to weigh some properties more than others via several criteria, giving the eventual weighting a valid backing. Another advantage of the process is that it provides any external user with a clear reasoning behind weighting decisions. The quantitative decision that is applied to each property for each application requirement is clearly stated, allowing an external user to gage how much they may agree/disagree with the rationale applied. Any selection process is subject to differences in opinion but increasing the number of these justifications ultimately allows the areas where these differences occur to be acknowledged rather than hidden.

Table 5 displays both the application requirements deemed to be of significant importance and the relevant material properties critical to the success of the pivoting-vane component under the conditions analysed thus far. Each of the application requirements in Table 5 deemed important is assigned a weight on a scale of between 1 and 10, which reflects their relative importance to the success of the device. A score of 1 means the requirement has the least significance to the success of the device and vice versa for a score of 10. The material properties are each evaluated against the above application requirements and given a score from 0-10, with 0 referring to a property which has no impact on the success of the requirement and 10 referring to that of the highest importance. The product of each requirement weight and material property weight are then summed for each application requirement to give a material property weighting factor.

The numerical values of the material properties of the materials under consideration are used to evaluate their relative strengths with respect to each other and represented in Table 6. To remove any element of operator opinion, the score for each material's property was based on a simple calculation through which the material with the most desirable numerical value was assigned a maximum score of ten. The remaining materials were then expressed as a percentage of the optimum value and factored to represent this percentage relative to a score of 10 e.g. a material property that was 80% of the best value, would receive a score of 8. This method allows any additional materials to be assessed by the same selection process, simply by expressing the new properties as a percentage of the best values. For the qualitative properties a fair rating was assigned a score of 4, good a score of 6 and excellent a score of 8.

Table 5. Material criteria and application requirement weighting table

		Affordable	Available	Consistent	Durable	Efficient	Responsive	Structural Integrity	Material Criteria Weight
	Weighted Importance	5	5	7	7	8	7	8	
	Material Criteria								
1	Corrosion Resistance	6	1	4	7	4	2	6	206
2	Creep Resistance	7	4	8	10	6	5	9	336
3	Yield Strength	4	6	6	8	6	4	7	280
4	Manufacturability	7	3	4	4	4	4	4	198
5	Melting Temperature	2	0	3	3	1	1	4	99
6	CoTE	2	0	9	6	7	6	7	269
7	UTS	4	0	4	6	4	3	8	207
8	Weight	5	0	5	5	7	9	5	254
9	Young's Modulus	3	0	6	6	6	3	6	216

Table 6. Material selection table

	Material Criteria	1	2	3	4	5	6	7	8	9	
	Material Criteria Weight	206	336	280	198	99	269	207	254	216	Total Score
Material	Nimonic 90	4.00	10.00	7.95	4.00	9.60	9.94	7.97	9.80	9.88	17101
	Nimonic 80A	6.00	5.43	8.42	4.00	9.57	9.94	6.60	9.79	10.00	15842
	Nimonic 81	8.00	3.76	5.81	4.00	9.64	9.88	6.60	9.95	9.59	14902
	Incoloy 864	8.00	3.12	2.03	4.00	9.76	9.42	1.98	10.00	8.35	12310
	IN X750/751	4.00	7.78	10.00	4.00	10.00	9.64	10.00	9.69	8.53	16986
	Inconel 600	4.00	1.75	1.74	6.00	9.90	10.00	3.30	9.47	9.65	11928

Based on the total score obtained for each material evaluated in Table 6, it is recommended that both Nimonic 90 and IN X750/751 be considered as strong candidates for the material required by the pivoting vane component. Nimonic 90 received a total score of 17101, the highest of the six materials considered and has superior 1000hr creep rupture properties, shown to be vital to the success of application. IN X750/751 received a total score of 16986, the second highest of the six materials and relatively identical to that demonstrated by Nimonic 90. Both Nimonic 90 and IN X750/751 have been shown to cope with the conditions predicted by this study, with 1000hr creep rupture properties capable of withstanding the maximum stresses to a minimum safety factor of 2. By contrast it has been demonstrated that IN 600, with a 1000hr creep rupture strength of just 38.6 MPa, would be insufficient at coping with the predicted conditions by the transient study. The yield strengths and ultimate tensile strengths for both Nimonic 90 and IN X750/751 far exceed that required by the application, which experiences a maximum stress of approximately 60 MPa.

The third highest scoring material was Nimonic 80A with a total score of 15842, approximately 8% lower than that of Nimonic 90. A factor that may be of merit to the possible success of Nimonic 80A is the increased levels of corrosion resistance over the two highest scoring alternatives. An in-house study appears to be the most comprehensive method of understanding the extent to which all three materials suffer from corrosion, and whether the improved performance of Nimonic 80A may warrant its preferred selection despite its

lower total score. The 1000hr creep rupture property of Nimonic 80A is also capable of withstanding the predicted conditions, in this instance to a maximum safety factor of 2.

The lower density and coefficient of thermal expansion may ultimately contribute to an eventual selection of Nimonic 90 as the preferred choice. However, elements of fatigue and cost still need to be considered before a final decision can be made. As mentioned, due to the relative lack of fatigue information it is recommended this comparison be performed in-house under conditions comparable to those in service.

Finally, unless it can be shown there are significant cost reductions to be made with Nimonic 81 and Incoloy 864, their lower respective scores of 14902 and 12310 make them unlikely choices in comparison to the their higher scoring alternatives.

Table 7 provide a summary of the most important material properties for some of the materials selected to be reviewed by this study. All properties are taken at 800℃ (unless stated otherwise) as a consequence of the common reference temperature stated in the manufacturer's technical data. While for this diesel engine application 800℃ was a satisfactory maximum temperature target for the simulation, with regards to fatigue strength, data concerning cycles of the order 1×10^9 were not available in the literature provided by the material manufacturers. Vane oscillation cycles of 1×10^9 or above are deemed to be close to the expected lifetime cycle count for the vane mechanism in a potential diesel engine application of ACT. Cycles closer to 1×10^6 and 1×10^8 are typically the maximum referenced, so analysing a materials' suitability with regards to fatigue is difficult. For the purpose of this study fatigue properties are not considered and as such are identified as an area of future work for consideration.

Table 7. Selected material properties

MATERIAL	Density (g/cm^3)	Melting Temperature (℃)	CoTE ($\mu m/m$℃)	750℃, 1000h Creep Rupture Strength (MPa)	Yield Strength (MPa)	UTS (MPa)
Inconel 600	8.47	1413	16.1	38.6	420(700℃)	250
Inconel X750/751	8.28	1427	16.7	172.0	560	758
Nimonic 80A	8.19	1365	16.2	210.0	580	500
Nimonic 90	8.18	1370	16.2	221.0	548	604

Nominal specific costs for IN 600 and IN X750 are £24/kg and £31/kg, respectively (Special Metals Corporation, 2002 and 2004). Costs for Nimonic 80A, 81 and 90 could not be retrieved but can be estimated by their composition. The cost for Nimonic 80A and 90 is estimated to similar to IN X750 due to their similar properties (MetalPrices, 2010).

As stated in Table 7, IN 600 has the lowest creep rupture strength compared to other materials. The simulation results showed a maximum stress of 58 MPa while IN 600 ruptures at 38.6 MPa at 750℃. The other materials showed an acceptable strength and Nimonic 90 has the highest among the rest of the materials.

In addition, Table 7 shows that IN X750 has highest coefficient of thermal expansion among the four materials. Higher thermal expansion is an important factor since expansion of the vanes could give rise to vane stickiness and therefore reliability of operation issues.

8. Conclusions

The presented work discussed the applicability and final selection of four material candidates for use in a turbocharger turbine nozzle for novel active control turbocharger (ACT). Since the concept of ACT involves the sinusoidal oscillation of the nozzle at a frequency equal to that emitted by the engine exhaust system (50Hz for this 10 litre diesel engine application at 2000 rpm) a very highly stressed component (the nozzle vane) had to be investigated for its mechanical integrity characteristics. The vane design employed was taken from an in-

house designed and built variable geometry turbocharger suitable for this type of engine (Rajoo, 2007). The work involved a CFD study followed by an FEA study to assist in the process of selection of the best amongst four superalloys identified as suitable candidates given the dynamic conditions existent at the turbocharger turbine inlet.

The difficulty and very substantial computational effort involved in setting up a fully transient CFD study with time-dependent rack position variation (sinusoidal profile of nozzle rack position of ACT) has meant a simplification of the process through a coarse discretisation of the pulse period time domain.

The transient study described predicted a maximum stress of 58.04 MPa, occurring at a vane angle of 70^0. In addition to the presentation of numerical values of time dependent maximum stresses, the work also provides descriptions of the factors which dictate the stress behaviour of the vane component. Variations in differential pressures between the pressure and suction sides of the vane have been shown to play a dominant role in the deformation behaviour of the component and become substantially more significant as the vane relative angle in relation to the absolute flow angle increases. It has also been shown that as a consequence, the vane at an angle of 70^0 commonly experiences maximum and global stresses a full order of magnitude higher than at angles of 40^0 and 55^0. For the majority of time per 0.02 s period the vane has been shown to exhibit stresses no greater than 10 MPa, which is encouraging with respect to fatigue life over the projected lifetime of the component (at over 10^9 cycles). The physical outputs of the transient study offer a robust compromise between a relatively fast steady-state simulation and a truly transient (flow and vane boundary condition) reality. Combining the multiple simulations has provided a general description of the conditions experienced by the pivoting vane component across a whole time period. With this information, the ability to select a material has been aided through a greater understanding of the range and variation of the stresses which must be withstood. Obtaining this variation and magnitude in stress levels has allowed identification of the peak stress levels within the time period which can be adequate in producing deformation by creep thus helping in the subsequent analysis and selection of the various superalloy material options.

The development of a material selection process has resulted in an unbiased approach to material evaluation with specific relevance to the application requirements. Improvements in density, coefficient of thermal expansion and creep resistance have resulted in Nimonic 90 scoring a slightly higher score of 17101 than the previously recommended material of IN X750/751, which obtained a total score of 16986. The choice between the two recommendations will ultimately come down to both fatigue properties and cost, factors which have not been considered and are recommended topics of possible future work. Improvements in corrosion resistance of both materials may need to be investigated through an in-house experimental study of the capabilities of both materials under application specific conditions to understand the levels of resistance required. As a consequence, the role of Nimonic 80A in providing a potential solution with superior corrosion resistance properties over Nimonic 90 and IN X750/751 should not be ignored.

9. References

1. European Commission (2010) Reducing CO2 emissions from light-duty vehicles [Online].Availablefrom: http://ec.europa.eu/environment/air/transport/co2/co2_home.htm
2. Martinez-Botas, R. and Pesiridis, A. (2007). Experimental evaluation of active flow control mixed-flow turbine for automotive turbocharger application. Journal of Turbomachinery. 129 p. 44–52.
3. Pesiridis, A., and Martinez-Botas, R., “Active Control Turbocharger for Automotive Application: An experimental evaluation”, Conference

Proceedings of the 8th International Conference on Turbocharging and Turbochargers, IMechE, London, 17-18 May 2006.
4. Rajoo, S. (2007) Steady and Pulsating Performance of a Variable Geometry Mixed Flow Turbocharger Turbine. Ph.D. Imperial College London
5. Honeywell (2010), Honeywell Turbo Technologies [Online]. Available from: http://www.honeywell.com/sites/ts/tt/
6. Arnold, S., Honeywell International Inc. (2004) Vane Design For Use In Variable Geometry Turbocharger. 6,672,059
7. Munz, S., Schmidt, P., Romuss, C., Brune, H. and Schiffer, H.P. (2007). Turbocharger for emission concepts with low-pressure-end exhaust-gas recirculation. [Online]. Available from: http://www.turbos.bwauto.com/service/default.aspx?doctype=12
8. Farag, M. (2008). Materials and Process Selection for Engineering Design. Boca Raton, USA: CRC Press
9. Mazur, Z., Luna-Ramírez, A., Juárez-Islas, J.A. and Campos-Amezcua, A. (2005). Failure analysis of a gas turbine blade made of Inconel 738LC alloy. Engineering Failure Analysis.[Online] 12 p. 474-486
10. Jovanovic, M. et al. (2005). Microstructure and mechanical properties of precision cast TiAl turbocharger wheel. Journal of Materials Processing Technology. 167 p. 14-21.
11. Shouren, W. et al. (2008). Centrifugal precision cast TiAl turbocharger wheel using ceramic mold. Journal of Materials Processing Technology. 204 p. 492-497.
12. Tetsui, T., Ono, S. (1999). Endurance and composition and microstructure effects on endurance of TiAl used in turbochargers. Intermetallics. 7 p. 689-697.
13. Zhang, W.J. et al. (2001). Physical properties of TiAl-base alloys. Scripta Materialia. 45 p. 645-651.
14. Tetsui, T. (2002). Development of a TiAl turbocharger for passenger vehicles. Materials Science & Engineering A. p. 582-588
15. Bocanegra-Bernal, M.H. and Matovic, B. (2010). Mechanical properties of silicon nitride based ceramics and its use in structural applications at high temperatures. Materials Science & Engineering A. 527 p. 1314-1338.
16. Sims, C., Stoloff, N. and Hagel, W. (eds.) (1987). Superalloys II. USA: John Wiley & Sons, Inc.
17. Dieter, G. (1997). Overview of the Materials Selection Process. In: ASM Handbook: Volume 20, Materials Selection and Design. ASM Handbooks Online.
18. Special Metals Corporation. (2002). INCONEL alloy 600. [Online]. Available from: http://www.specialmetals.com/products/index.php
19. Special Metals Corporation. (2004). INCONEL alloy X-750. [Online]. Available from: http://www.specialmetals.com/products/index.php
20. Special Metals Corporation. (2004). INCONEL alloy 751. [Online]. Available from: http://www.specialmetals.com/products/index.php
21. Special Metals Corporation. (2004). INCOLOY 864. [Online]. Available from: http://www.specialmetals.com/products/index.php
22. MetalPrices (2010) Rhenium [Online]. Available from: http://www.metalprices.com/FreeSite/metals/re/re.asp